Original Article

Deep learning-based reconstruction enhances image quality and improves diagnosis in magnetic resonance imaging of the shoulder joint

Zijun Liu[1]^, Baohong Wen[1], Ziyu Wang[1], Kaiyu Wang[2], Lizhi Xie[2], Yimeng Kang[1], Qiuying Tao[1], Weijian Wang[1], Yong Zhang[1], Jingliang Cheng[1], Yan Zhang[1]

[1]Department of Magnetic Resonance Imaging, the First Affiliated Hospital of Zhengzhou University, Zhengzhou, China; [2]MR Research China, GE Healthcare, Beijing, China

Contributions: (I) Conception and design: Z Liu, K Wang; (II) Administrative support: B Wen, L Xie; (III) Provision of study materials or patients: Z Liu, B Wen; (IV) Collection and assembly of data: Z Liu, Z Wang, Q Tao; (V) Data analysis and interpretation: Z Liu, Y Kang; (VI) Manuscript writing: All authors; (VII) Final approval of manuscript: All authors.

Correspondence to: Yan Zhang, MD. Department of Magnetic Resonance Imaging, the First Affiliated Hospital of Zhengzhou University, 1 Jianshe East Road, Zhengzhou 450052, China. Email: fcczhangy61@zzu.edu.cn.

Background: Accelerated magnetic resonance imaging sequences reconstructed using the vendor-provided Recon deep learning algorithm (DL-MRI) were found to be more likely than conventional magnetic resonance imaging (MRI) sequences to detect subacromial (SbA) bursal thickening. However, the extent of this thickening was not extensively explored. This study aimed to compare the image quality of DL-MRI with conventional MRI sequences reconstructed via conventional pipelines (Conventional-MRI) for shoulder examinations and evaluate the effectiveness of DL-MRI in accurately demonstrating the degree of SbA bursal and subcoracoid (SC) bursal thickening.

Methods: This prospective cross-sectional study enrolled 41 patients with chronic shoulder pain who underwent 3-T MRI (including both Conventional-MRI and accelerated MRI sequences) of the shoulder between December 2022 and April 2023. Each protocol consisted of oblique axial, coronal, and sagittal images, including proton density-weighted imaging (PDWI) with fat suppression (FS) and oblique coronal T1-weighted imaging (T1WI) with FS. The image quality and degree of artifacts were assessed using a 5-point Likert scale for both Conventional-MRI and DL-MRI. Additionally, the degree of SbA and SC bursal thickening, as well as the relative signal-to-noise ratio (rSNR) and relative contrast-to-noise ratio (rCNR) were analyzed using the paired Wilcoxon test. Statistical significance was defined as $P<0.05$.

Results: The utilization of accelerated sequences resulted in a remarkable 54.7% reduction in total scan time. Overall, DL-MRI exhibited superior image quality scores and fewer artifacts compared to Conventional-MRI. Specifically, DL-MRI demonstrated significantly higher measurements of SC bursal thickenings in the oblique sagittal PDWI sequence compared to Conventional-MRI [3.92 (2.83, 5.82) *vs.* 3.74 (2.92, 5.96) mm, $P=0.028$]. Moreover, DL-MRI exhibited higher detection of SbA bursal thickenings in the oblique coronal PDWI sequence [2.61 (1.85, 3.46) *vs.* 2.48 (1.84, 3.25) mm], with a notable trend towards significant differences ($P=0.071$). Furthermore, the rSNRs of the muscle in DL-MRI images were significantly higher than those in Conventional-MRI images across most sequences ($P<0.001$). However, the rSNRs of bone on Conventional-MRI of oblique axial and oblique coronal PDWI sequences showed adverse results [oblique axial: 1.000 (1.000, 1.000) *vs.* 0.444 (0.367, 0.523); and oblique coronal: 1.000 (1.000, 1.000)

^ ORCID: 0009-0002-8794-3476.

vs. 0.460 (0.387, 0.631); all P<0.001]. Additionally, all DL-MRI images exhibited significantly greater rSNRs and rCNRs compared to accelerated MRI sequences reconstructed using traditional pipelines (P<0.001).

Conclusions: In conclusion, the utilization of DL-MRI enhances image quality and improves diagnostic capabilities, making it a promising alternative to Conventional-MRI for shoulder imaging.

Keywords: Shoulder magnetic resonance imaging (shoulder MRI); deep learning (DL); image quality; subacromial bursa (SbA bursa); subcoracoid bursa (SC bursa)

Submitted Oct 09, 2023. Accepted for publication Feb 13, 2024. Published online Mar 15, 2024.
doi: 10.21037/qims-23-1412
View this article at: https://dx.doi.org/10.21037/qims-23-1412

Introduction

Magnetic resonance imaging (MRI) is widely acknowledged as a highly effective technique for diagnosing structural abnormalities in the shoulder joint, due to its exceptional ability to capture detailed soft tissue images (1,2). However, the lengthy scan times associated with shoulder MRI examinations can pose challenges for patient compliance, especially in individuals experiencing shoulder pain. Additionally, these extended scan times increase the susceptibility to artifacts caused by breathing or involuntary movement, thereby significantly compromising image quality and diagnostic accuracy.

Currently, routine sequences based on fast spin-echo (FSE), such as T1-weighted imaging (T1WI), proton density-weighted imaging (PDWI), and T2-weighted imaging (T2WI), are commonly employed in shoulder imaging. However, these sequences are prone to artifacts (3), further hindering the accuracy of the diagnostic process.

Reducing acquisition time in shoulder imaging not only improves patient comfort, particularly for those experiencing shoulder pain, but also minimizes the occurrence of artifacts in the resulting images. Two techniques that have shown promise in achieving faster scanning are compressed SENSE (C-SENSE) and parallel imaging (PI). While both techniques offer time-saving benefits, some studies revealed that SENSitivity Encoding (SENSE), a PI technique, has been surpassed by C-SENSE in terms of reducing acquisition time (4,5). However, it is important to note that these techniques often come with a trade-off, namely a potential sacrifice in signal-to-noise ratio (SNR) to achieve faster scanning (6). This means that the image quality may be compromised to some extent, as the SNR is a critical factor in obtaining clear and accurate diagnostic information.

Recent advancements in deep learning (DL) have led to the development of convolutional neural networks (CNN) that significantly accelerate the image reconstruction process for conventional MRI sequences. Unlike traditional reconstruction pipelines, these DL-based CNN models disrupt the trade-off between scan time and image quality, allowing for the optimization of image contrast while simultaneously reducing scan duration and image noise (7-10). Accelerated MRI sequences reconstructed using the vendor-provided Recon deep learning algorithm (DL-MRI) techniques have proven to be highly beneficial in clinical routine scans, with previous investigations successfully utilizing them to evaluate various musculoskeletal systems (10-13). These studies have demonstrated the remarkable potential of DL in speeding up scanning procedures and enhancing overall image quality.

Changes in bursal thickness can indicate different shoulder pathologies, with the most common being bursitis. There is literature indicating that for patients with bursitis of different degrees of bursa thickening, the treatment effect of the same treatment method varies (14). Shoulder pain is commonly associated with bursal effusion, a pathological characteristic. Subacromial (SbA) bursitis, an inflammation of the SbA bursa, is a common cause of shoulder pain (15-17). Additionally, studies have suggested that isolated subcoracoid (SC) bursitis may also contribute to shoulder pain (18). Measuring the thickness of the SbA and *SC* bursa in shoulder imaging is clinically valuable for diagnosing, monitoring, planning treatments, and predicting outcomes related to various shoulder pathologies. For the treatment of bursitis, physical therapy or injection of anti-inflammatory agents are typically used as conservative treatments in mild to moderate cases. If bursitis progresses to the chronic stage, it can damage surrounding structures, worsen the condition, and lead to tendinopathy or even tendon rupture. Therefore, it is crucial to utilize imaging techniques to accurately assess the thickness of the bursal and evaluate

whether the treatment methods have improved the patient's condition.

In a previous study, DL-MRI sequences were found to be more effective than traditional MRI sequences in detecting SbA bursal thickening, although the extent of this thickening was not extensively explored (19). Assessing the degree of thickness in the intra-articular bursa can provide valuable insights into the severity of the patient's condition, as it often correlates with the level of shoulder pain experienced. However, there is a lack of studies evaluating the effectiveness of DL sequences in assessing the degree of SbA and SC bursa thickening in patients with shoulder pain.

The objective of this study is to investigate the differences in image quality between DL-MRI and conventional MRI sequences, as well as to evaluate the role of DL-MRI sequences in accurately demonstrating the degree of SbA bursa and SC bursa thickening. By comparing the image quality of DL-MRI sequences with traditional MRI sequences, we aim to determine the potential benefits of DL-MRI in enhancing the visualization and assessment of bursal thickening. We present this article in accordance with the STROBE reporting checklist (available at https://qims.amegroups.com/article/view/10.21037/qims-23-1412/rc).

Methods

This prospective cross-sectional study was permitted by the Review Committee of the First Affiliated Hospital of Zhengzhou University (No. 2023-KY-0888-003) and was conducted in accordance with the Declaration of Helsinki (as revised in 2013). Written informed consent was obtained from each included patient. Data for this study were extracted from an IRB approved larger prospective study. DL-MRI and conventional MRI were sequentially acquired within one examination only. We transparently communicated the scientific objectives and relevance of the research to patients, emphasizing its potential to enhance future medical services like reduction in examination time, alleviation of discomfort experienced by patients enduring headaches, neck pain, shoulder pain during the imaging process and potential enhancements in image quality. Patients were informed about potential benefits of participation, including complimentary MRI examinations and the opportunity to gain medical knowledge. Importantly, patients were thoroughly informed about the risks associated with repeated MRI examinations, ensuring their understanding and voluntary acceptance towards participating in the study. Ethical standards were rigorously followed, with patients providing informed consent that encompassed a clear understanding of all aspects of the research.

Patients

The sample-size in this study was selected according to the literature from Kaniewska *et al.* (19). To determine the minimal sample size, an a priori power analysis was conducted with an effect size of 0.5, an alpha error of 0.05, and a beta error of 0.2. For data with a Laplace distribution, a minimum sample size of 23 patients was required.

Between December 2022 and April 2023, we prospectively gathered data from 49 patients with shoulder pain at the First Affiliated Hospital of Zhengzhou University. The study focused on those with chronic shoulder pain, explicitly excluding cases of acute pain due to fractures or similar acute conditions. Eligibility for inclusion also required patients to provide informed consent voluntarily. Specific exclusion criteria were applied to ensure the quality and relevance of the data. These included: (I) inadequate magnetic resonance images, (II) patients who had undergone shoulder surgery, and (III) the presence of a shoulder tumor.

Ultimately, our study comprised of 41 participants. The median age was 53.0 years [interquartile range (IQR): 47.5–58.5 years], with 11 males and 30 females. Twenty-three participants had issues with the right shoulder, and 18 participants had issues with the left. The distribution of bursitis was 18 in the SbA bursa and 30 in the SC bursa. A flow chart providing a detailed breakdown of this information is available in *Figure 1*.

MRI acquisition

The experiments were conducted using a 3T GE MRI scanner (SIGNATM Premier, GE Healthcare, Waukesha, WI, USA) equipped with a dedicated 16-channel shoulder coil. The acquisition routine for shoulder MRI involved three types of sequences: conventional MRI sequences reconstructed using conventional pipelines (referred to as Conventional-MRI), accelerated MRI sequences reconstructed using the vendor-provided Recon DL algorithm (referred to as DL-MRI), and accelerated MRI sequences reconstructed without using the vendor-provided Recon DL algorithm (referred to as Non-DL-MRI). Each sequence consisted of oblique axial, coronal, and sagittal images, including PDWI with fat suppression (FS) and

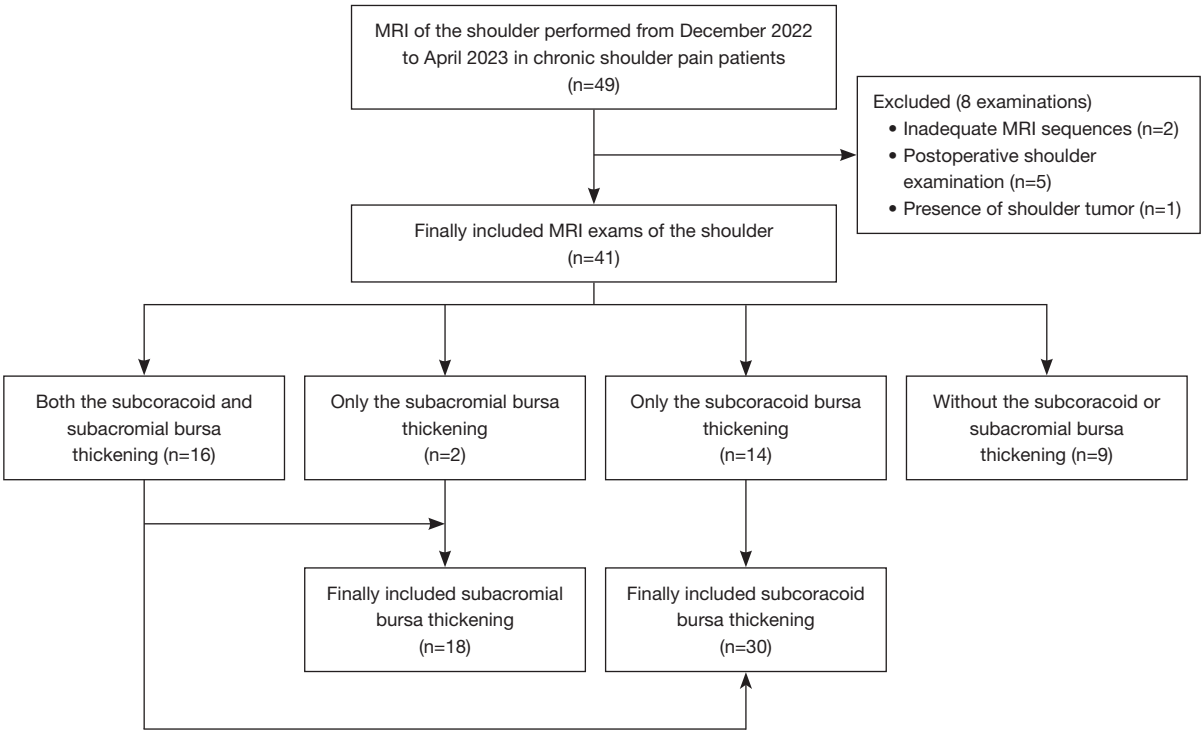

Figure 1 Flow diagram of patient selection. MRI, magnetic resonance imaging.

oblique coronal images T1WI with FS.

Detailed MRI parameters of conventional MRI sequences and accelerated MRI sequences are shown in *Table 1*.

DL image reconstruction

A Recon DL pipeline prototype (7) was utilized to obtain DL images in this study. This pipeline employs a deep CNN to reconstruct MR images, resulting in improved SNR, sharper edges, and reduced truncation artifacts. The CNN is integrated into the standard reconstruction process, allowing for adjustable noise reduction levels ranging from 0 to 100%. This ensures that the DL images have reduced noise variance based on the chosen noise reduction level. Additionally, the network is capable of recognizing truncation artifacts and employs de-ringing techniques to enhance image sharpness. In this study, we used a noise reduction level of 75%. The CNN in this reconstruction incorporates more than 10,000 kernels and over 4.4 million trainable parameters. It was trained using supervised learning, with the training data comprising of high-resolution MRI images that were nearly perfect, as well as low-resolution versions synthesized using established methods. To enhance the network's robustness, image enhancement techniques such as rotation, flipping, intensity gradients, phase manipulation, and additional Gaussian noise were employed during the training process. The network is also capable of recognizing Gibbs ringing near sharp edges and implements de-ringing to improve image sharpness.

Qualitative assessment of image quality

Both the Conventional-MRI and DL-MRI sequences were assessed for image quality and the presence of artifacts using a 5-point Likert scale (0, poor; 1, light; 2, medium; 3, good and 4, perfect). The following were the specific scoring criteria used for the assessment:

- Image quality on a 5-point scale (0= Non-diagnostic image quality: a lot of noise and it is almost impossible to analyze the contour of the structure; 1= Poor-diagnostic image quality: a lot of noise, have significantly distorted contours of the analyzed structures; 2= Relatively good diagnostic image quality: easy-to-observe image noise retains

Table 1 MRI parameters of conventional MRI sequences and accelerated MRI sequences

Parameters	Conventional MRI sequences				Accelerated MRI sequences			
	OSag PD FS	OCor PD FS	OCor T1w FS	OAx PD FS	OSag PD FS	OCor PD FS	OCor T1w FS	OAx PD FS
TE (ms)	41.1 (40.1–41.5)	41.6 (39.9–42.0)	10.4 (10.1–10.4)	42.3 (41.0–43.7)	41.7 (40.1–42.3)	42.5 (39.9–42.5)	7.7 (7.3–7.7)	43.3 (41.0–45.4)
TR (ms)	3,375 (2,757–3,411)	3,090 (2,470–3,090)	317 (312–318)	3,025 (2,727–3,477)	2,853 (2,757–2,889)	2,605 (2,470–2,605)	516 (516–579)	2,669 (2,545–3,100)
Thickness (mm)	4.00	4.00	4.00	4.00	4.00	4.00	4.00	4.00
Matrix	384×256	384×256	384×256	384×288	384×256	384×256	384×256	384×288
Field of view (mm^2)	160×160	160×160	160×160	180×180	160×160	160×160	160×160	180×180
Flip angle (°)	111	111	111	111	111	111	111	111
Number of excitation	2.00	2.00	2.00	2.00	1.00	1.00	1.00	1.00
Acquisition time (min:s)	02:15 (01:32–02:48)	02:04 (01:32–02:34)	01:22 (01:19–01:26)	02:16 (01:31–2:47)	00:58 (00:47–01:11)	01:01 (00:48–01:13)	00:42 (00:38–0:48)	00:55 (00:44–01:07)

TE and TR data were represented by setting parameters (scanning the actual parameter range). Acquisition time data represented as average value (minimum, maximum). MRI, magnetic resonance imaging; OSag, oblique sagittal; PD, proton density; FS, fat suppression; OCor, oblique coronal; T1w, T1-weighted imaging; OAx, oblique axial; TE, echo time; TR, repetition time.

the contour of the shoulder joint structure with significant but non-interfering inhomogeneity; 3= Good diagnostic image quality: the image noise is low, but the description of the analyzed structure is very good and there is no significant inhomogeneity; 4= Excellent image quality: with high image sharpness, without very significant image noise, and perfectly describing the structure under analysis, without any inhomogeneity or signal variation.)

- Artifacts on a 5-point scale (0= Severe artifacts affect the evaluation of anatomical structures; 1= Moderate artifacts moderately affected the evaluation of anatomical structures; 2= Mild or moderate artifacts mildly affected the evaluation of anatomical structures; 3= Mild artifacts were observed but did not affect the evaluation of anatomical structures; 4= No obvious artifacts.)

Two experienced radiologists (B.W. and Y.Z., with 10 and 25 years' experience of joint MRI, respectively) independently evaluated the images for image quality and artifact severity in a blind and randomized manner. Prior to evaluation, the radiologists familiarized themselves with the image rating criteria. Interobserver agreement was assessed separately, and the mean scores for DL-MRI and Conventional-MRI image quality, as well as artifact severity, were compared.

Quantitative assessment of the image quality

To evaluate the effectiveness of DL-MRI sequences in demonstrating the degree of SbA bursa and SC bursa thickening, two readers independently measured the maximum thickness of these bursae on the oblique coronal and sagittal fat-suppressed PDWI images.

To conduct a quantitative assessment of image quality, two readers independently selected a round-shaped region of interest (ROI) measuring 4 mm^2 in both the bone (humeral head, excluding any edematous areas) and muscle (deltoid, excluding any edematous areas) within each set of images. The signal intensity (SI) within the measured ROI and the standard deviation (STD) of the SI within the measured ROI were recorded by each reader. To determine the relative signal-to-noise ratio (rSNR) and relative contrast-to-noise ratio (rCNR) for each batch of images, the mean values of SI and STD determined by the two readers were utilized. By comparing rSNR and rCNR, quantitative analyses were performed to compare Conventional-MRI and DL-MRI, as well as Non-DL-MRI and DL-MRI, respectively.

The following methods were used for each relative metric (10):

rSNR:

$$rSNR = \max Norm\left(\frac{SI}{STD}\right) \quad [1]$$

rCNR:

$$rCNR = \max Norm\left(\frac{\left|SI_{muscle} - SI_{bone}\right|}{mean\left(STD_{bone}, STD_{muscle}\right)}\right) \quad [2]$$

where SI is the signal of the given ROI, STD is the standard deviation within the ROI, and:

$$\max Norm\left(f_i\right) = \frac{f_i}{\max\left(\forall f_i\right)} \quad [3]$$

Statistical analysis

Statistical analyses were performed using IBM SPSS Statistics (version 25.0, IBM corporation). Graphs were generated using GraphPad Prism version 9.5.1 for Windows (GraphPad Software, San Diego, California USA, www.graphpad.com). The study employed two-sided P values, and statistical significance was determined at a significance level of P<0.05. Continuous data were assessed for normality using the Kolmogorov-Smirnov test or Shapiro-Wilk test, depending on the sample size, and were presented as mean ± standard deviation (SD) or median (IQR), as appropriate. Categorical variables were reported as numbers (%). Paired Wilcoxon signed-rank tests were utilized to compare differences in image quality, artifact severity, rSNR, and rCNR between different quantification techniques. To evaluate the consistency of interpretations between the two readers, the intraclass correlation coefficient (ICC) was calculated. The ICC was interpreted as follows: <0.2 = poor, 0.21–0.50 = fair, 0.51–0.60 = moderate, 0.61–0.75 = good, and 0.75–1.00 = excellent.

Results

Scan time

The accelerated sequence significantly reduced the total scan time, with an average of just 3 minutes and 36 seconds, representing a remarkable 54.7% decrease compared to the regular sequence. In contrast, the regular sequence required an average total scan duration of 7 minutes and 57 second.

Image quality

Figure 2 visually demonstrates the disparity between DL-MRI and Conventional-MRI images, clearly highlighting that DL-MRI images exhibit fewer artifacts and superior image quality compared to Conventional-MRI images. To provide a comprehensive evaluation, *Table 2* presents the subjective image quality and artifacts severity scores for both image sets, along with the ICC between the two readers.

The image quality scores of oblique coronal FS PDWI for DL-MRI [3.00 (3.00, 3.25)] were found to be comparable to those of Conventional-MRI [3.50 (3.00, 4.00)] (P=0.326). However, DL-MRI exhibited superior image quality scores overall compared to Conventional-MRI for oblique axial FS PDWI [3.50 (3.00, 4.00)], oblique sagittal FS PDWI [4.00 (3.00, 4.00)], and oblique coronal FS T1WI [4.00 (4.00, 4.00)]. These differences were statistically significant (all P<0.001). The ICC analysis revealed that the image quality scores of DL-MRI were consistent across the two readers, with ICC values ranging from 0.760 to 0.806. In contrast, the ICC analysis for Conventional-MRI ranged from 0.521 to 0.691, which indicated a relatively lower inter-observer agreement in image quality scores. These findings suggest that DL-MRI exhibits improved inter-observer agreement and consistency in image quality assessment.

All DL-MRI images exhibited significantly higher artifacts scores compared to Conventional-MRI. Specifically, oblique axial FS PDWI [3.00 (3.00, 4.00)], oblique sagittal FS PDWI [3.50 (3.00, 4.00)], oblique coronal FS T1WI [4.00 (3.00, 4.00)], and oblique coronal FS PDWI [3.50 (3.00, 4.00)] of DL-MRI had significantly higher artifacts scores than their counterparts in Conventional-MRI [oblique axial FS PDWI, 3.00 (2.50, 3.00); oblique sagittal FS PDWI, 3.00 (3.00, 3.50); oblique coronal FS T1WI, 3.00 (3.00, 4.00); and oblique coronal FS PDWI, 3.00 (3.00, 3.50)] (all P=0.001). The results indicated that DL-MRI images exhibit a lower occurrence of artifacts compared to Conventional-MRI images. The consistency of artifact scores in DL-MRI was evaluated using the ICC analysis, which yielded a range of 0.768 to 0.858, indicating a high level of agreement between the two readers. Conversely, the ICC analysis for Conventional-MRI yielded a range of 0.618 to 0.673, suggesting a relatively lower level of agreement between the two readers. These findings suggest that DL-MRI not only reduces artifacts but also enhances

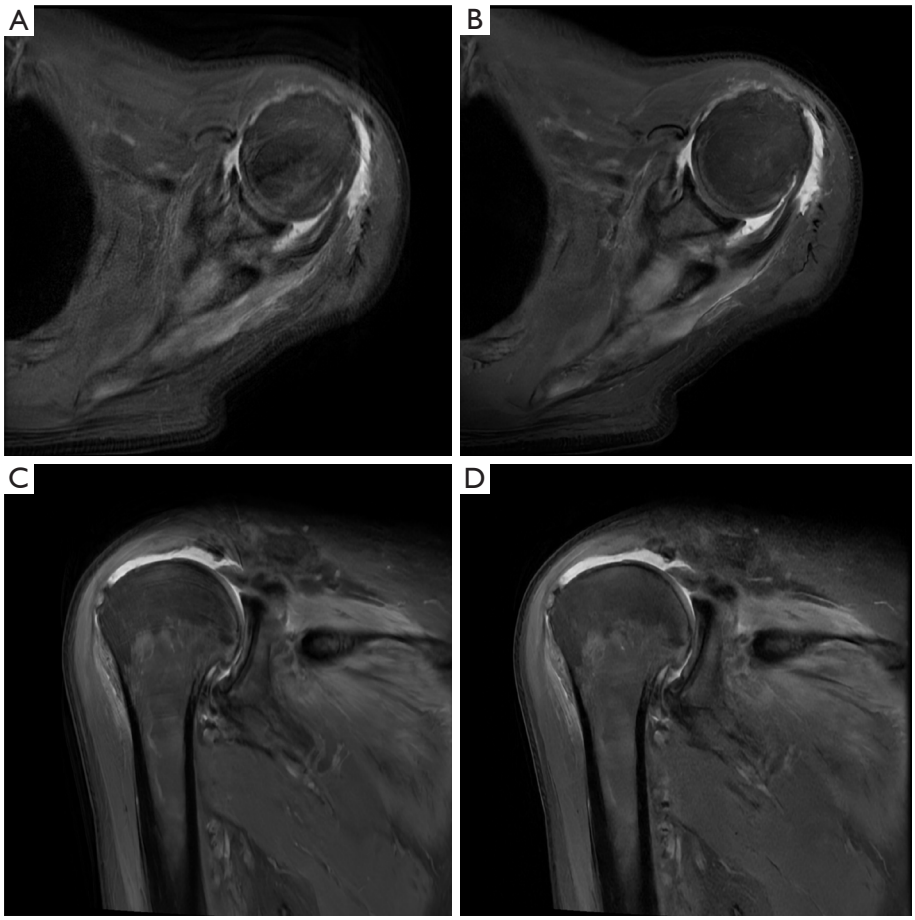

Figure 2 MRI of a 67-year-old man with left shoulder pain. (A-D) MRI include oblique axial/coronal PDWI with FS standard images reconstructed using conventional pipelines (A,C), accelerated image with DLR (B,D). Conventional sequences reconstructed using conventional pipelines (A,C) show artifacts and noise. Accelerated images with DLR (B,D) show decreased noise and increased sharpness. MRI, magnetic resonance imaging; PDWI, proton density-weighted imaging; FS, fat-saturated; DLR, deep learning-based reconstruction.

interobserver agreement.

Bursa thickness

Table 3 presents the evaluation of SbA bursa and SC bursa thickening using DL-MRI and Conventional-MRI. The comparison of bursa thickness between the SC bursa and SbA bursa, as observed in Conventional-MRI and DL-MRI, is illustrated in *Figure 3*. The findings suggest that DL-MRI has a higher likelihood of detecting bursa thickening compared to Conventional-MRI.

The measurements of SC bursa thickening on DL-MRI images [oblique coronal FS PDWI: 4.14 (2.46, 5.70) mm; oblique sagittal FS PDWI: 3.92 (2.83, 5.82) mm] were found to be higher compared to Conventional-MRI images. Notably, the difference in thickness became statistically significant in the oblique sagittal FS PDWI (P=0.028). Similarly, the measurements of SbA bursa thickening on DL-MRI images [2.61 (1.85, 3.46) mm] were higher than those on Conventional-MRI images [2.48 (1.84, 3.25) mm] in the oblique coronal FS PDWI. Although the difference did not reach statistical significance, the P value of 0.071 suggests a trend towards significance. In the oblique sagittal FS PDWI, the measurements of SbA bursa thickening on DL-MRI images [2.64 (1.44, 3.21) mm] were observed to be slightly lower compared to Conventional-MRI images [2.75 (1.77, 3.11) mm]. However, this difference was not statistically significant (P=0.983). *Figures 4* and *5* visually depict the contrasting effects of DL-MRI and Conventional-MRI in visualizing SbA and SC bursa

Table 2 Subjective image quality and artifacts severity scores

Sequences	Parameters	Scores (comparison individually)			Interobserver agreement	
		DL-MRI	Conventional-MRI	P	Conventional-MRI	DL-MRI
Oblique axial FS PDWI	Subjective image quality	3.50 [3.00, 4.00]	3.00 [2.50, 3.00]	<0.001*	0.623	0.760
	Artifacts	3.00 [3.00, 4.00]	3.00 [2.50, 3.00]	0.001*	0.673	0.768
Oblique coronal FS PDWI	Subjective image quality	3.00 [3.00, 3.25]	3.50 [3.00, 4.00]	0.326	0.691	0.782
	Artifacts	3.50 [3.00, 4.00]	3.00 [3.00, 3.50]	0.001*	0.618	0.794
Oblique coronal FS T1WI	Subjective image quality	4.00 [4.00, 4.00]	3.00 [3.00, 3.00]	<0.001*	0.521	0.778
	Artifacts	4.00 [3.00, 4.00]	3.00 [3.00, 4.00]	0.001*	0.670	0.858
Oblique sagittal FS PDWI	Subjective image quality	4.00 [3.00, 4.00]	3.00 [2.50, 3.00]	<0.001*	0.546	0.806
	Artifacts	3.50 [3.00, 4.00]	3.00 [3.00, 3.50]	0.001*	0.623	0.775

The data for the scores for image quality and artifact severity were shown as median [upper quartile, lower quartile]. *, P value with significance. DL-MRI, accelerated magnetic resonance imaging sequences reconstructed using the vendor-provided Recon deep learning algorithm; Conventional-MRI, conventional magnetic resonance imaging sequences reconstructed using conventional pipelines; FS, fat suppression; PDWI, proton density-weighted imaging; T1WI, T1-weighted imaging.

Table 3 Degree of subacromial bursa and subcoracoid bursa thickening

Sequences	Parameters	Thickening, mm (comparison individually)			Interobserver agreement	
		DL-MRI	Conventional-MRI	P	Conventional-MRI	DL-MRI
Oblique coronal FS PDWI	Subacromial bursa	2.61 [1.85,3.46]	2.48 [1.84,3.25]	0.071	0.985	0.987
	Subcoracoid bursa	4.14 [2.46,5.70]	3.47 [2.17,5.22]	0.122	0.995	0.995
Oblique sagittal FS PDWI	Subacromial bursa	2.64 [1.44,3.21]	2.75 [1.77,3.11]	0.983	0.993	0.990
	Subcoracoid bursa	3.92 [2.83,5.82]	3.74 [2.92,5.96]	0.028*	0.991	0.997

The data for the thickening of the subacromial bursa and subcoracoid bursa were shown as median [upper quartile, lower quartile]. *, P value with significance. DL-MRI, accelerated magnetic resonance imaging sequences reconstructed using the vendor-provided Recon deep learning algorithm; Conventional-MRI, conventional magnetic resonance imaging sequences reconstructed using conventional pipelines; FS, fat suppression; PDWI, proton density-weighted imaging.

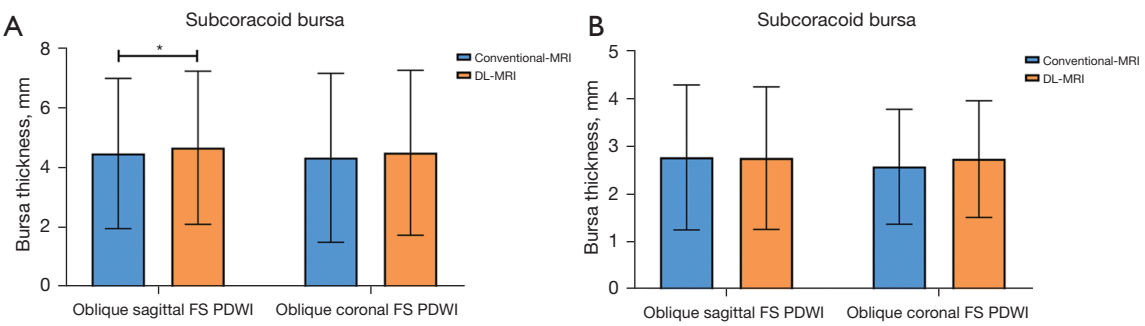

Figure 3 Comparison of the bursa thickness in Conventional-MRI and DL-MRI. (A) Comparison of the bursa thickness of subcoracoid bursa in Conventional-MRI and DL-MRI. (B) Comparison of the bursa thickness of subacromial bursa in Conventional-MRI and DL-MRI. *, P value with significance. Conventional-MRI, conventional magnetic resonance imaging sequences reconstructed using conventional pipelines; DL-MRI, accelerated magnetic resonance imaging sequences reconstructed using the vendor-provided Recon deep learning algorithm; FS, fat suppression; PDWI, proton density-weighted imaging.

Figure 4 MRI of a 55-year-old woman with right shoulder pain. (A-D) MRI images include oblique coronal/sagittal PDWI with FS standard images reconstructed using conventional pipelines (A,C), accelerated image with DLR (B,D). Conventional sequences reconstructed using conventional pipelines (A,C) show artifacts and noise, and the subacromial bursa thickenings measured in the oblique coronal FS PDWI was 2.54 mm (A) and in the oblique sagittal FS PDWI was 2.75 mm (C). Accelerated images with DLR (C,D) show decreased noise and increased sharpness, and the subacromial bursa thickenings measured in the oblique coronal FS PDWI was 3.21 mm (B) and in the oblique sagittal FS PDWI was 3.21 mm (D). MRI, magnetic resonance imaging; PDWI, proton density-weighted imaging; FS, fat-saturated; DLR, deep learning-based reconstruction.

thickenings. Specifically, *Figure 4* demonstrates that the SbA bursa thickness measured in Conventional-MRI was lower than that in DL-MRI, both in the oblique coronal FS PDWI and the oblique sagittal FS PDWI. Furthermore, our analysis revealed that the SC bursa thickening measured in Conventional-MRI was comparatively smaller than that in DL-MRI, as depicted in *Figure 5* for both the oblique coronal FS PDWI and the oblique sagittal FS PDWI. It is worth noting that the degree of bursal thickening showed similar values across DL-MRI (ranging from 0.987 to 0.997) and Conventional-MRI (ranging from 0.985 to 0.995) images, indicating a consistent level of thickening. Moreover, both DL-MRI and Conventional-MRI demonstrated strong interobserver agreement in assessing bursal thickening.

Comparison of rSNR and rCNR

Figure 6 provides an intuitive visualization of the comparison between Conventional-MRI and DL-MRI, as well as Non-DL-MRI and DL-MRI, in terms of rSNR and rCNR. The differences are clearly depicted in the figure. Based on the findings presented in *Table 4*, the rSNRs of bone on Conventional-MRI of oblique axial FS PDWI [1.000

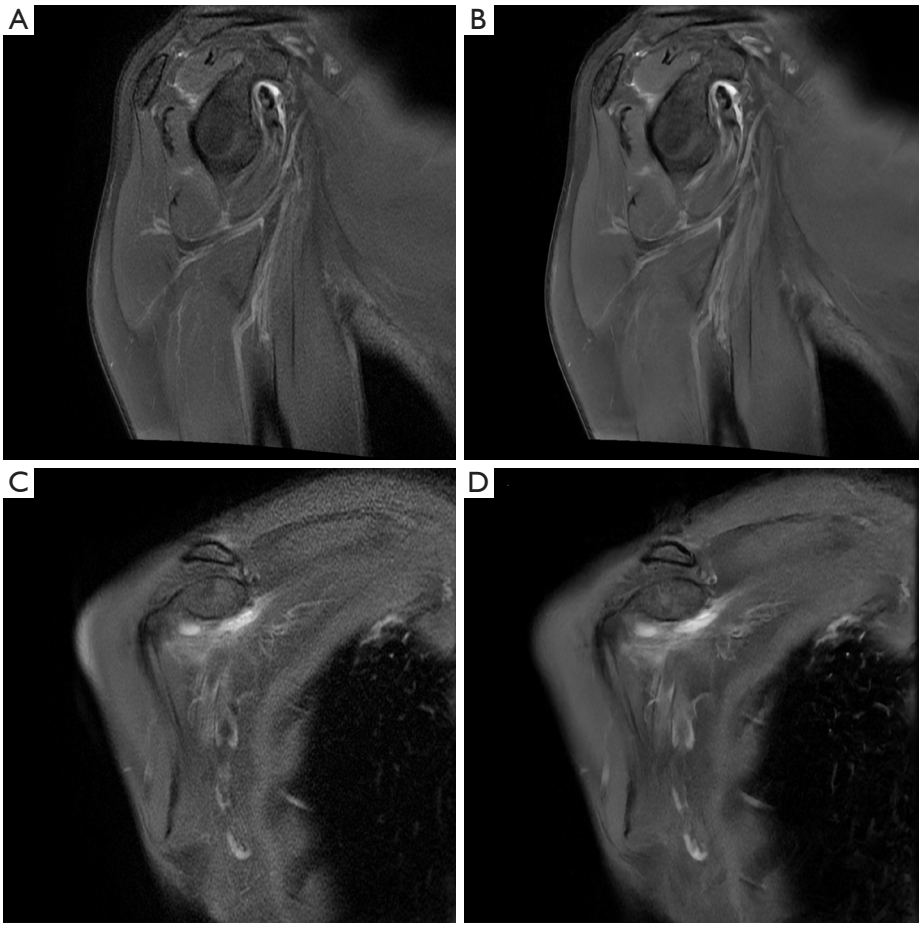

Figure 5 MRI of a 51-year-old woman with right shoulder pain. (A-D) MRI include oblique sagittal/coronal PDWI with FS standard images reconstructed using conventional pipelines (A,C), accelerated image with DLR (B,D). Conventional sequences reconstructed using conventional pipelines (A,C) show artifacts and noise, and the subcoracoid bursa thickenings measured in the oblique sagittal FS PDWI was 2.68 mm (A) and in the oblique coronal FS PDWI was 3.87 mm (C). Accelerated images with DLR (B,D) show decreased noise and increased sharpness, and the subcoracoid bursa thickenings measured in the oblique sagittal FS PDWI was 2.91 mm (B) and in the oblique coronal FS PDWI was 4.40 mm (D). MRI, magnetic resonance imaging; PDWI, proton density-weighted imaging; FS, fat-saturated; DLR, deep learning-based reconstruction.

(1.000, 1.000)] and oblique coronal FS PDWI [1.000 (1.000, 1.000)] images were significantly higher compared to DL-MRI [oblique axial FS PDWI: 0.444 (0.367, 0.523); oblique coronal FS PDWI: 0.460 (0.387, 0.631)] (all P<0.001). Furthermore, the rSNRs of bone on oblique coronal FS T1WI with DL [1.000 (0.811, 1.000)] and oblique sagittal FS PDWI [1.000 (1.000, 1.000)] images were significantly higher compared to Conventional-MRI [oblique coronal FS T1WI: 0.827 (0.617, 1.000); oblique sagittal FS PDWI: 0.747 (0.574, 0.972)] (P=0.036, P<0.001, respectively). In terms of bone imaging, our analysis revealed that DL-MRI and Conventional-MRI images exhibited comparable noise reduction abilities.

Additionally, our analysis revealed that the rSNRs of the muscle in DL-MRI images were significantly higher than those in Conventional-MRI images across all sequences (all P<0.001), except for the oblique coronal FS PDWI (P=0.464). Furthermore, in the oblique axial/coronal FS PDWI sequences (all P<0.001), as well as the oblique coronal FS T1WI (P=0.028), the rCNRs of DL-MRI images were significantly higher compared to Conventional-MRI images. However, in the case of the oblique sagittal FS PDWI, the difference in rCNR did not reach statistical significance (P=0.091).

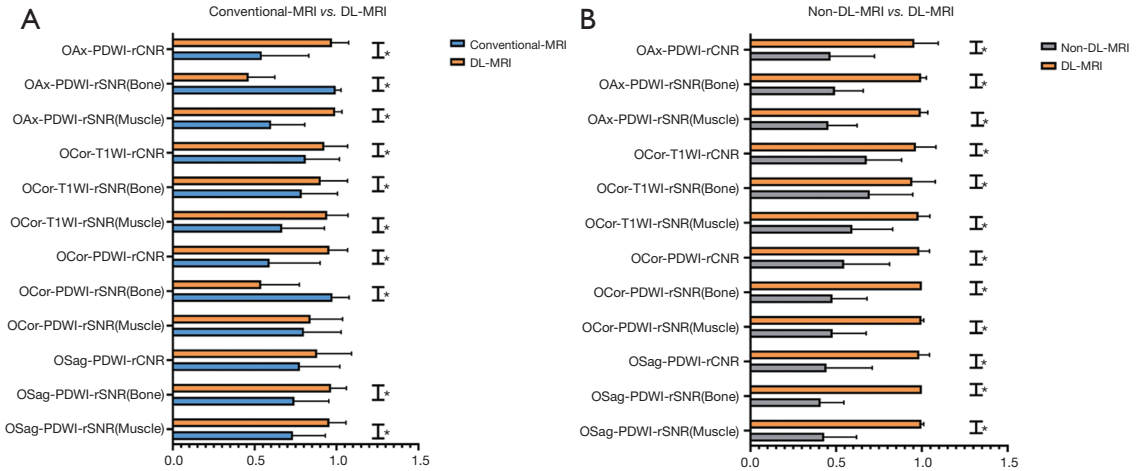

Figure 6 Comparison of rSNR and rCNR between different sequence images. (A) Comparison of rSNR and rCNR between Conventional-MRI and DL-MRI. (B) Comparison of rSNR and rCNR between Non-DL-MRI and DL-MRI. *, P value with significance. OAx, oblique axial; PDWI, proton density-weighted imaging; rCNR, relative contrast-to-noise ratio; rSNR, relative signal-to-noise ratio; OCor, oblique coronal; T1WI, T1-weighted imaging; OSag, oblique sagittal; Conventional-MRI, conventional magnetic resonance imaging sequences reconstructed using conventional pipelines; DL-MRI, accelerated magnetic resonance imaging sequences reconstructed using the vendor-provided Recon deep learning algorithm; Non-DL-MRI, accelerated magnetic resonance imaging sequences reconstructed without using the vendor-provided Recon deep learning algorithm.

Table 4 Results of quantitative comparison of bone and muscle between DL-MRI and Conventional-MRI on different sequences

Sequences	Parameters	rSNR				rCNR			
		Conventional-MRI	DL-MRI	Z	P	Conventional-MRI	DL-MRI	Z	P
Oblique axial FS PDWI	Bone	1.000 [1.000, 1.000]	0.444 [0.367, 0.523]	−5.553	<0.001*	0.483 [0.318, 0.744]	1.000 [1.000, 1.000]	−4.970	<0.001*
	Muscle	0.567 [0.461, 0.748]	1.000 [1.000, 1.000]	−5.371	<0.001*	–	–	–	–
Oblique coronal FS PDWI	Bone	1.000 [1.000, 1.000]	0.460 [0.387, 0.631]	−5.034	<0.001*	0.596 [0.343, 0.884]	1.000 [1.000, 1.000]	−4.529	<0.001*
	Muscle	0.935 [0.604, 1.000]	1.000 [0.656, 1.000]	−0.732	0.464	–	–	–	–
Oblique coronal FS T1WI	Bone	0.827 [0.617, 1.000]	1.000 [0.811, 1.000]	−2.093	0.036*	0.885 [0.672, 1.000]	1.000 [0.947, 1.000]	−2.196	0.028
	Muscle	0.658 [0.417, 0.991]	1.000 [0.977, 1.000]	−3.959	<0.001*	–	–	–	–
Oblique sagittal FS PDWI	Bone	0.747 [0.574, 0.972]	1.000 [1.000, 1.000]	−4.296	<0.001*	0.866 [0.566, 1.000]	1.000 [0.844, 1.000]	−1.691	0.091
	Muscle	0.699 [0.593, 0.952]	1.000 [1.000, 1.000]	−4.140	<0.001*	–	–	–	–

The data for rSNR and rCNR were shown as median [upper quartile, lower quartile]. *, P value with significance. DL-MRI, accelerated magnetic resonance imaging sequences reconstructed using the vendor-provided Recon deep learning algorithm; Conventional-MRI, conventional magnetic resonance imaging sequences reconstructed using conventional pipelines; rSNR, relative signal-to-noise ratio; rCNR, relative contrast-to-noise ratio; FS, fat suppression; PDWI, proton density-weighted imaging; T1WI, T1-weighted imaging.

Table 5 Results of quantitative comparison of bone and muscle between DL-MRI and Non-DL-MRI on different sequences

Sequences	Parameters	rSNR				rCNR			
		Non-DL-MRI	DL-MRI	Z	P	Non-DL-MRI	DL-MRI	Z	P
Oblique axial FS PDWI	Bone	0.441 [0.382, 0.605]	1.000 [1.000, 1.000]	−5.553	<0.001*	0.441 [0.296, 0.589]	1.000 [1.000, 1.000]	−4.957	<0.001*
	Muscle	0.426 [0.358, 0.548]	1.000 [1.000, 1.000]	−5.566	<0.001*	–	–	–	–
Oblique coronal FS PDWI	Bone	0.436 [0.312, 0.599]	1.000 [1.000, 1.000]	−5.527	<0.001*	0.439 [0.351, 0.775]	1.000 [1.000, 1.000]	−4.671	<0.001*
	Muscle	0.442 [0.315, 0.583]	1.000 [1.000, 1.000]	−5.553	<0.001*	–	–	–	–
Oblique coronal FS T1WI	Bone	0.628 [0.470, 0.987]	1.000 [1.000, 1.000]	−3.738	<0.001*	0.665 [0.539, 0.837]	1.000 [1.000, 1.000]	−4.464	<0.001*
	Muscle	0.560 [0.377, 0.753]	1.000 [1.000, 1.000]	−5.216	<0.001*	–	–	–	–
Oblique sagittal FS PDWI	Bone	0.369 [0.312, 0.508]	1.000 [1.000, 1.000]	−5.579	<0.001*	0.360 [0.255, 0.622]	1.000 [1.000, 1.000]	−5.384	<0.001*
	Muscle	0.382 [0.299, 0.485]	1.000 [1.000, 1.000]	−5.553	<0.001*	–	–	–	–

The data for rSNR and rCNR were shown as median [upper quartile, lower quartile]. *, P value with significance. DL-MRI, accelerated magnetic resonance imaging sequences reconstructed using the vendor-provided Recon deep learning algorithm; Non-DL-MRI, accelerated magnetic resonance imaging sequences reconstructed without using the vendor-provided Recon deep learning algorithm; rSNR, relative signal-to-noise ratio; rCNR, relative contrast-to-noise ratio; FS, fat suppression; PDWI, proton density-weighted imaging; T1WI, T1-weighted imaging.

In terms of both bone and muscle, all DL-MRI images exhibited significantly higher rSNRs compared to the original accelerated MRI images, as determined by a non-parametric test (paired Wilcoxon test; all P<0.001), as shown in *Table 5*. Additionally, our study demonstrated that all DL-MRI images had significantly greater rCNRs compared to Non-DL-MRI images (all P<0.001), as indicated in *Table 5*.

Discussion

In our study, we found that it was plausible to consider DL-MRI as a potential substitution for Conventional-MRI in shoulder MRI examinations because of the superior image quality of DL-MRI compared to Conventional-MRI in the majority of cases, as well as the enhanced efficacy of DL-MRI in evaluating the degree of SbA bursa and SC bursa thickenings. Given that DL-MRI is particularly valuable in detecting SbA and SC bursa thickenings, we also speculate that it has potential in identifying and characterizing specific shoulder lesions.

MRI is a valuable tool for accurately and comprehensively evaluating various shoulder anatomical structures, such as the extent of tendons, the muscles of the rotator cuff, and the glenohumeral joint capsule (20-22). However, the conventional sequences used in shoulder MRI often require a significant amount of time to complete. This prolonged duration can cause discomfort for patients experiencing pain and may also lead to the presence of artifacts in the resulting images. To address these challenges, this study introduces a DL technique aimed at reducing the examination time for shoulder MRI by 54.7%. By leveraging DL, the goal was to explore whether reconstructed accelerated images, with 75% noise reduction, can serve as a superior substitute for conventional-MRI images in shoulder MRI examinations.

Previous research has indicated that DL-MRI has the potential to generate images of higher quality compared to Conventional-MRI in the FS PDWI and FS T2WI sequences (23). Besides, Dratsch *et al.* (24) have assessed the image quality of shoulder MRI utilizing a combination of compressed sensing (CS) acquisition and DL reconstruction. It has been confirmed that the DL-based algorithm allows for additional acceleration of acquisition time compared

to conventional methods. Notably, the reconstruction in this study involved super-resolution reconstruction by DL following the undersampling of K-space data through CS, a crucial aspect in reducing acquisition time. A significant technical challenge associated with this technology pertains to the reliability of the information in post-production increments. The DL reconstruction we employed primarily focused on image denoising. The reduction in acquisition time is incidental and resulted from the improved noise reduction capability, leading to a potential decrease in number of excitation (NEX). Concurrently, additional research, inspired by Kaniewska *et al.* (19), explores whether DL-MRI holds advantages in delineating the thickness of the SbA and SC bursa. Nevertheless, in anatomical structures like bones and joints, the absence of appropriate third-party standards as reference poses a challenge. DL technology in these areas requires further validation, necessitating future studies with suitable samples, such as *in vitro* investigations.

In our study, we observed that DL-MRI images generally exhibited significantly better image quality than Conventional-MRI images, and also required shorter examination times. Specifically, DL-MRI performed comparably to Conventional-MRI in terms of image quality for oblique coronal FS PDWI. These findings align with previous research, suggesting that DL-MRI consistently offers superior image quality compared to Conventional-MRI.

Our investigation revealed a notable difference in artifact scores between DL-MRI and Conventional-MRI, with DL-MRI exhibiting significantly higher scores (P=0.001) compared to conventional MRI (11). This disparity could potentially be attributed to the differences in acquisition time between our study and the literature referenced.

In a study conducted by Kaniewska *et al.*, it was demonstrated that the use of faster periodically rotated overlapping parallel lines with enhanced reconstruction (PROPELLER) sequences, combined with DL post-processing, resulted in superior image quality and higher diagnostic confidence compared to traditional PROPELLER sequences (19). Additionally, the DL sequences were found to be more effective in detecting bursal thickening that went unnoticed by the traditional PROPELLER sequences. However, it is important to note that Kaniewska *et al.* did not perform precise numerical measurements of the thickened bursa. To further investigate the effectiveness of DL sequences in detecting bursa thickening, our study focused on evaluating the thickening of the SbA and SC bursa using oblique coronal/sagittal FS PDWI images. Our findings indicate that the measurements of SC thickenings on DL-MRI images were consistently higher compared to Conventional-MRI images. This difference reached statistical significance in the oblique sagittal FS PDWI sequence (P=0.028). Additionally, in the oblique coronal FS PDWI sequence, the measurements of SbA thickenings on DL-MRI images were higher than those on Conventional-MRI images, with a P value of 0.071, indicating a tendency toward significance. However, it is important to note that the measurements of SC thickenings on DL-MRI images were higher than those on Conventional-MRI images in the oblique coronal FS PDWI sequence. Conversely, the measurements of SbA thickenings on DL-MRI images were lower than those on Conventional-MRI images in the oblique sagittal FS PDWI sequence. Despite these observations, neither of these differences reached statistical significance. The limited number of participants in our study, coupled with the prevalence of significant bursa effusions among them, may have influenced our results. Consequently, both DL-MRI and Conventional-MRI images exhibited evident bursal sac hypertrophy, making it challenging to discern subtle thickness differences. To obtain more conclusive findings, further research is warranted, preferably with larger sample sizes and a broader range of disease severity among patients. Based on our current findings, we believe that DL-MRI has the potential to provide clearer visualization of SbA and SC thickness, thereby enhancing the precision of disease diagnosis. However, to validate this assertion and fully understand the benefits of DL-MRI in clinical practice, additional studies involving more diverse patient populations are necessary.

Previous studies have reported improvements in SNR and CNR when utilizing DL techniques in both phantom experimental experiments and clinical evaluations (7,25). To assess the noise reduction capabilities of DL-MRI compared to Conventional-MRI, we calculated the rSNR and rCNR. Furthermore, we quantitatively compared DL-MRI to Non-DL-MRI in terms of noise reduction capabilities using rSNR and rCNR. Our experimental results demonstrated that the accelerated sequence images reconstructed using DL (75%) exhibited higher rSNR and rCNR values compared to the accelerated sequence images without DL in every image. These differences were statistically significant (P<0.001), aligning with the findings of a previous study (10).

Besides, in the oblique axial FS PDWI and oblique

coronal FS PDWI images, Conventional-MRI exhibited higher relative rSNRs of bone compared to DL-MRI (all P<0.001). Conversely, in the oblique coronal FS T1WI and oblique sagittal FS PDWI images, DL-MRI demonstrated greater rSNRs of bone than Conventional-MRI (P=0.036, P<0.001, respectively). Therefore, in terms of bone imaging, the noise reduction capabilities of DL-MRI and Conventional-MRI were found to be comparable. In addition, our study revealed that the rSNRs of muscle in DL-MRI images were consistently higher than those in Conventional-MRI images across all sequences. These differences reached statistical significance (all P<0.001), except for the oblique coronal FS PDWI sequence (P=0.464). These findings suggest that the DL technique is more effective at reducing noise in muscle tissue compared to bone tissue. This discrepancy may be attributed to the inherent differences in noise distributions between muscle and bone tissues in MRI images. Muscle tissue typically exhibits lower noise levels with a relatively uniform signal distribution. This uniformity aids in mitigating the impact of noise, leading to higher image quality. In contrast, bone tissue imaging may have higher noise levels due to its lower SI in MRI images and its complex structure, which includes numerous small details and gaps. These intricate features within the bone structure can contribute to variations in noise levels, making it more challenging for the DL technique to effectively reduce noise in bone tissue. The image results obtained from our study highlight the limitations of the DL technique, as it cannot completely eliminate noise or infinitely improve the SNR. There exists a threshold beyond which further improvements become challenging to achieve. Furthermore, our findings indicated that in the oblique axial/coronal FS PDWI sequences (all P<0.001) and oblique coronal FS T1WI sequence (P=0.028), the rCNRs of DL-MRI images were significantly higher compared to Conventional-MRI images. However, in the oblique sagittal FS PDWI sequence, the difference in rCNRs between DL-MRI and Conventional-MRI images did not reach statistical significance (P=0.091). Based on these observations, it can be inferred that, DL tends to exhibit greater rCNRs than Conventional images in most cases.

Previous research has explored the application of DL reconstruction technology in shoulder MRI, demonstrating its efficacy in reducing acquisition times. Similarly, studies focusing on knee MRI have shown that DL-MRI has the potential to shorten scan times, suggesting that DL-MRI can serve as a viable alternative to Conventional-MRI (23,26). Moreover, DL-MRI has exhibited remarkable performance in various anatomical regions, including the pituitary, temporomandibular joint, prostate, and brain (7,27-29). These studies have demonstrated the versatility and effectiveness of DL across different tissues in MRI, as well as in different imaging modality (30,31), further highlighting its potential as a valuable tool in medical imaging.

There are several limitations in our study that should be acknowledged. Firstly, the small sample size and limited diversity of lesions prevented us from fully validating the clinical diagnostic efficacy of DL-MRI in various shoulder diseases. Though the primary objective of this study was to investigate the potential of DL-MRI as a replacement for conventional sequences in routine shoulder MRI scanning, the limited sample diversity could restrict the applicability of the results across various shoulder conditions. Secondly, despite efforts to ensure unbiased evaluation by having readers assess the images blindly and in a random order, variations in noise patterns may have led to different interpretations of image types among the readers. Addressing this issue in future studies, such as standardizing noise patterns or implementing additional measures to minimize reader bias, may be crucial for ensuring more reliable and objective evaluations of image quality. Thirdly, due to the lack of arthroscopy or other reference standards, especially the lack of accuracy assessment for bursal measurements with an external reference standard, we relied solely on conventional images as the reference standard. This limitation may have impacted the accuracy and comprehensiveness of our findings. Furthermore, our current evaluation focused solely on objectively assessing the denoising capabilities of DL-MRI in different tissue types (muscle *vs.* bone). Further exploration is needed to fully understand the capabilities and limitations of this technique in a clinical setting.

Conclusions

DL-MRI presents itself as a superior alternative to the conventional sequence for shoulder MRI. This is due to its ability to significantly reduce scan time by approximately 54.7%, while simultaneously enhancing image quality and improving the consistency of reader interpretations. Moreover, DL-MRI proves to be particularly valuable in the detection of SbA and SC, offering a more pronounced visualization of these pathologies. By adopting DL-MRI in shoulder MRI protocols, healthcare providers can benefit

from the substantial time savings without compromising the diagnostic accuracy or quality of the images. The improved image quality and consistency of reader interpretations further contribute to enhanced diagnostic confidence and potentially better patient outcomes. Furthermore, the enhanced detection of SbA and SC thickenings through DL-MRI underscores its potential to aid in the identification and characterization of specific shoulder pathologies, that can enable more targeted and effective treatment strategies.

Acknowledgments

We express our gratitude to all individuals who have provided assistance and support throughout the course of this study. Their contributions have been invaluable and greatly appreciated.
Funding: None.

Footnote

Reporting Checklist: The authors have completed the STROBE reporting checklist. Available at https://qims.amegroups.com/article/view/10.21037/qims-23-1412/rc

Conflicts of Interest: All authors have completed the ICMJE uniform disclosure form (available at https://qims.amegroups.com/article/view/10.21037/qims-23-1412/coif). K.W. and L.X. are employees of GE Healthcare. The other authors have no conflicts of interest to declare.

Ethical Statement: The authors are accountable for all aspects of the work in ensuring that questions related to the accuracy or integrity of any part of the work are appropriately investigated and resolved. The study was conducted in accordance with the Declaration of Helsinki (as revised in 2013). The study was approved by the Review Committee of the First Affiliated Hospital of Zhengzhou University (No. 2023-KY-0888-003), and informed consent was taken from all individual participants.

References

1. Small KM, Adler RS, Shah SH, Roberts CC, Bencardino JT, Appel M, Gyftopoulos S, Metter DF, Mintz DN, Morrison WB, Subhas N, Thiele R, Towers JD, Tynus KM, Weissman BN, Yu JS, Kransdorf MJ. ACR Appropriateness Criteria(®) Shoulder Pain-Atraumatic. J Am Coll Radiol 2018;15:S388-402.
2. Nacey NC, Geeslin MG, Miller GW, Pierce JL. Magnetic resonance imaging of the knee: An overview and update of conventional and state of the art imaging. J Magn Reson Imaging 2017;45:1257-75.
3. Ogul H, Taydas O, Sakci Z, Altinsoy HB, Kantarci M. Posterior shoulder labrocapsular structures in all aspects; 3D volumetric MR arthrography study. Br J Radiol 2021;94:20201230.
4. Niitsu M, Saruya S, Sakaguchi K, Watarai K, Yoneyama M, Katsumata Y, Inoue K, Kozawa E. Motion-robust MR imaging of the shoulder using compressed SENSE MultiVane. Eur J Radiol Open 2022;9:100450.
5. L. Geerts-Ossevoort, E. de Weerdt, A. Duijndam, G. van IJperen, H. Peeters, M. Doneva, M. Nijenhuis, A. Huang. Compressed SENSE. Speed done right. Every time. (2018) Available online: https://philipsproductcontent.blob.core.windows.net/assets/20180109/619119731f2a42c4acd4a863008a46c7.pdf
6. Obama Y, Ohno Y, Yamamoto K, Ikedo M, Yui M, Hanamatsu S, Ueda T, Ikeda H, Murayama K, Toyama H. MR imaging for shoulder diseases: Effect of compressed sensing and deep learning reconstruction on examination time and imaging quality compared with that of parallel imaging. Magn Reson Imaging 2022;94:56-63.
7. Lebel RM. Performance characterization of a novel deep learning-based MR image reconstruction pipeline. arXiv: 2008.06559.
8. Yaman B, Hosseini SAH, Moeller S, Ellermann J, Uğurbil K, Akçakaya M. Self-supervised physics-based deep learning MRI reconstruction without fully-sampled data. 2020 IEEE 17th International Symposium on Biomedical Imaging (ISBI), Iowa City, IA, USA, 2020:921-5.
9. Kim M, Kim HS, Kim HJ, Park JE, Park SY, Kim YH, Kim SJ, Lee J, Lebel MR. Thin-Slice Pituitary MRI with Deep Learning-based Reconstruction: Diagnostic Performance in a Postoperative Setting. Radiology 2021;298:114-22.

10. Koch KM, Sherafati M, Arpinar VE, Bhave S, Ausman R, Nencka AS, Lebel RM, McKinnon G, Kaushik SS, Vierck D, Stetz MR, Fernando S, Mannem R. Analysis and Evaluation of a Deep Learning Reconstruction Approach with Denoising for Orthopedic MRI. Radiol Artif Intell 2021;3:e200278.
11. Hahn S, Yi J, Lee HJ, Lee Y, Lim YJ, Bang JY, Kim H, Lee J. Image Quality and Diagnostic Performance of Accelerated Shoulder MRI With Deep Learning-Based Reconstruction. AJR Am J Roentgenol 2022;218:506-16.
12. Kidoh M, Shinoda K, Kitajima M, Isogawa K, Nambu M, Uetani H, Morita K, Nakaura T, Tateishi M, Yamashita Y, Yamashita Y. Deep Learning Based Noise Reduction for Brain MR Imaging: Tests on Phantoms and Healthy Volunteers. Magn Reson Med Sci 2020;19:195-206.
13. Shanbhogue K, Tong A, Smereka P, Nickel D, Arberet S, Anthopolos R, Chandarana H. Accelerated single-shot T2-weighted fat-suppressed (FS) MRI of the liver with deep learning-based image reconstruction: qualitative and quantitative comparison of image quality with conventional T2-weighted FS sequence. Eur Radiol 2021;31:8447-57.
14. Lee DH, Hong JY, Lee MY, Kwack KS, Yoon SH. Relation Between Subacromial Bursitis on Ultrasonography and Efficacy of Subacromial Corticosteroid Injection in Rotator Cuff Disease: A Prospective Comparison Study. Arch Phys Med Rehabil 2017;98:881-7.
15. Urwin M, Symmons D, Allison T, Brammah T, Busby H, Roxby M, Simmons A, Williams G. Estimating the burden of musculoskeletal disorders in the community: the comparative prevalence of symptoms at different anatomical sites, and the relation to social deprivation. Ann Rheum Dis 1998;57:649-55.
16. Skazalski C, Bahr R, Whiteley R. Shoulder complaints more likely in volleyball players with a thickened bursa or supraspinatus tendon neovessels. Scand J Med Sci Sports 2021;31:480-8.
17. Luime JJ, Koes BW, Hendriksen IJ, Burdorf A, Verhagen AP, Miedema HS, Verhaar JA. Prevalence and incidence of shoulder pain in the general population; a systematic review. Scand J Rheumatol 2004;33:73-81.
18. Schraner AB, Major NM. MR imaging of the subcoracoid bursa. AJR Am J Roentgenol 1999;172:1567-71.
19. Kaniewska M, Deininger-Czermak E, Getzmann JM, Wang X, Lohezic M, Guggenberger R. Application of deep learning-based image reconstruction in MR imaging of the shoulder joint to improve image quality and reduce scan time. Eur Radiol 2023;33:1513-25.
20. Bachmann GF, Melzer C, Heinrichs CM, Möhring B, Rominger MB. Diagnosis of rotator cuff lesions: comparison of US and MRI on 38 joint specimens. Eur Radiol 1997;7:192-7.
21. Zanetti M, Gerber C, Hodler J. Quantitative assessment of the muscles of the rotator cuff with magnetic resonance imaging. Invest Radiol 1998;33:163-70.
22. Fields BKK, Skalski MR, Patel DB, White EA, Tomasian A, Gross JS, Matcuk GR Jr. Adhesive capsulitis: review of imaging findings, pathophysiology, clinical presentation, and treatment options. Skeletal Radiol 2019;48:1171-84.
23. Liu J, Li W, Li Z, Yang J, Wang K, Cao X, Qin N, Xue K, Dai Y, Wu P, Qiu J. Magnetic resonance shoulder imaging using deep learning-based algorithm. Eur Radiol 2023;33:4864-74.
24. Dratsch T, Siedek F, Zäske C, Sonnabend K, Rauen P, Terzis R, Hahnfeldt R, Maintz D, Persigehl T, Bratke G, Iuga A. Reconstruction of shoulder MRI using deep learning and compressed sensing: a validation study on healthy volunteers. Eur Radiol Exp 2023;7:66.
25. Kim M, Kim HS, Park JE, Park SY, Kim YH, Kim SJ, Lee J, Lebel MR. Thin-Slice Pituitary MRI with Deep Learning-Based Reconstruction for Preoperative Prediction of Cavernous Sinus Invasion by Pituitary Adenoma: A Prospective Study. AJNR Am J Neuroradiol 2022;43:280-5.
26. Recht MP, Zbontar J, Sodickson DK, Knoll F, Yakubova N, Sriram A, et al. Using Deep Learning to Accelerate Knee MRI at 3 T: Results of an Interchangeability Study. AJR Am J Roentgenol 2020;215:1421-9.
27. Wen BH, Liu ZJ, Zhang Y, Cheng JL. Using deep learning to accelerate temporomandibular joint MRI at 3 T: A case report. Asian J Surg 2023;46:4110-1.
28. Ueda T, Ohno Y, Yamamoto K, Murayama K, Ikedo M, Yui M, Hanamatsu S, Tanaka Y, Obama Y, Ikeda H, Toyama H. Deep Learning Reconstruction of Diffusion-weighted MRI Improves Image Quality for Prostatic Imaging. Radiology 2022;303:373-81.
29. Estler A, Hauser TK, Mengel A, Brunnée M, Zerweck L, Richter V, Zuena M, Schuhholz M, Ernemann U, Gohla G. Deep Learning Accelerated Image Reconstruction of Fluid-Attenuated Inversion Recovery Sequence in Brain Imaging: Reduction of Acquisition Time and Improvement of Image Quality. Acad Radiol 2024;31:180-6.
30. Heinrich A, Yücel S, Böttcher B, Öner A, Manzke M, Klemenz AC, Weber MA, Meinel FG. Improved image quality in transcatheter aortic valve implantation planning CT using deep learning-based image reconstruction.

Quant Imaging Med Surg 2023;13:970-81.
31. Lei L, Zhou Y, Guo X, Wang L, Zhao X, Wang H, Ma J, Yue S. The value of a deep learning image reconstruction algorithm in whole-brain computed tomography perfusion in patients with acute ischemic stroke. Quant Imaging Med Surg 2023;13:8173-89.

Cite this article as: Liu Z, Wen B, Wang Z, Wang K, Xie L, Kang Y, Tao Q, Wang W, Zhang Y, Cheng J, Zhang Y. Deep learning-based reconstruction enhances image quality and improves diagnosis in magnetic resonance imaging of the shoulder joint. Quant Imaging Med Surg 2024;14(4):2840-2856. doi: 10.21037/qims-23-1412

